Electronic Supplementary Material (ESI) for Nanoscale.

Supplementary Information

Chirality-dependent densities of carbon nanotubes by in situ 2D fluorescence-excitation and Raman characterisation in a density gradient after ultracentrifugation.

Sofie Cambré, Pieter Muyshondt, Remi Federicci and Wim Wenseleers

1. Density Calibration.

To determine the density of the different fractions after DGU, we prepared well-calibrated solutions of a known density (determined using a pycnometer) and measured their absorption spectra. The gradient medium shows a characteristic absorption peak at 2285nm (well separated from the SWCNT absorption bands and another reason why D_2O is used instead of H_2O). Using the well-calibrated solutions of known density, the intensity of this absorption peak can be directly related to the density of the solutions.

The pycnometer was calibrated at a temperature of 20±0.3ºC using H_2O (ρ=0.9982±0.00013g/mL). As such, the density of the D_2O used was determined to be 1.10570±0.00015g/mL, and a 37.2% m/m Nycodenz solution in D_2O was found to have a density of 1.33579±0.00018g/mL.

Furthermore, the DGU also redistributes the H_2O-content (present as a minor impurity in the D_2O) in the different fractions. By measuring the absorption spectra of known concentrations of H_2O in D_2O, the H_2O-content in each fraction could be obtained and the densities were corrected for this.

For each of the SWCNT fractions, an absorption spectrum was measured and weighted reference spectra of Nycodenz and H_2O (with known concentration) were subtracted so that the characteristic absorption of the Nycodenz and H_2O disappears from the absorption spectrum (see Figure S1). The error on the concentration of Nycodenz and H_2O thus obtained results in a maximum error of 0.002g/mL on the densities.

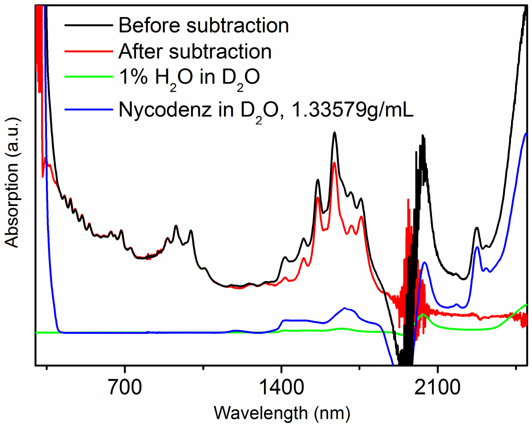

Figure S1: Absorption spectrum of an example SWCNT fraction obtained from the centrifuge tube after DGU (black) and the spectrum (red) after subtracting the weighted reference absorption spectra (those of H_2O (green) and Nycodenz (blue)), to eliminate their characteristic absorption bands. The absorption of pure D_2O was subtracted during the measurement. These specific amounts were then used to calculate the densities of each specific fraction.

To illustrate the relation of the obtained distributions as a function of density to the original data as a function of position in the centrifuge tube, we re-plot here Figure 4 from the main text, with a secondary axis denoting height (or depth) in the centrifuge tube on top (negative, relative to the liquid-air meniscus). It should be noted however, that, because of the slightly different gradients (height-to-density calibrations) used for the separation of DOC and SC-suspended SWCNTs, the height-scale cannot be directly compared between both experiments.

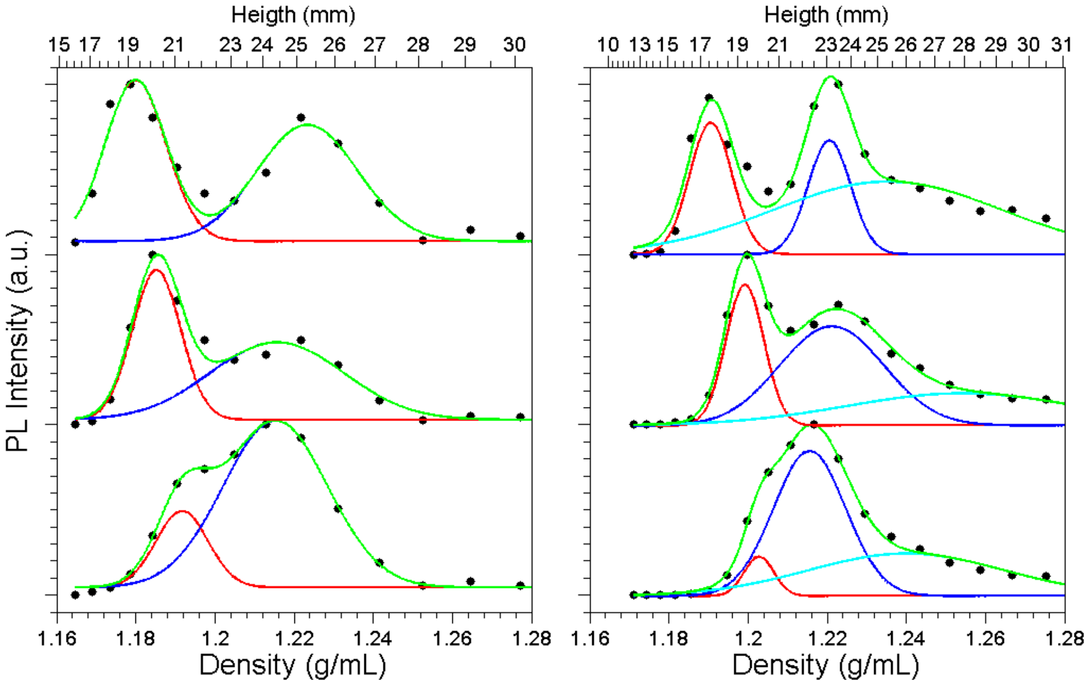

Figure S2: PLE intensity for different chiralities as a function of density (bottom axis) and height (top axis) in the centrifuge tube in 2% DOC (left panel) or 2% SC (right panel), From top to bottom: (9,8), (10,5) and (7,6). (See also Figure 4 in the main text).

2. Fraction selection

We prepared in each centrifuge run at least one reference sample, prepared identically in the other centrifuge tubes and manually selected fractions (~60-80µL) from these centrifuge tubes directly after the ultracentrifugation. The fractions were selected with 1-2mm distances between them so that densities of different fractions are not mixed. A typical example of a centrifuge tube after DGU and the selection of the fractions can be found in Figure 1.

Note that the densities are thus not determined inside the same DGU tube as the actual *in situ* measurements are performed. The reason for this is that the gradient medium diffuses at a much faster rate than the SWCNTs (smaller molecule) and therefore determining the densities after the *in situ* measurements would not give reliable results (see section 3).

To test the accuracy of the densities obtained in this way, i.e. including the accuracy of manually selecting the fractions, we prepared two reference samples and collected the fractions in the same way. Figure S2 presents the so-obtained density versus height curves, from which it is clear that within the relevant range of 5-25mm, densities are perfectly reproducible within the experimental error of 0.002g/mL, and therefore we aimed at separating the SWCNTs in this central region of the centrifuge tube. The top of the centrifuge tube (0 mm) and the bottom of the centrifuge tube (30 mm) deviate slightly (0.002 and 0.007g/mL in this specific example) since the density varies much more steeply in these particular regions. When fitting the density curve with a polynomial of degree 2, maximum deviations from the polynomial to the experimental data points are approx. 0.002g/mL. Therefore, measuring in the appropriate height region of the centrifuge tube (~5-25mm) and fitting the data points, we assume an accuracy of our density calibration of 0.002g/mL.

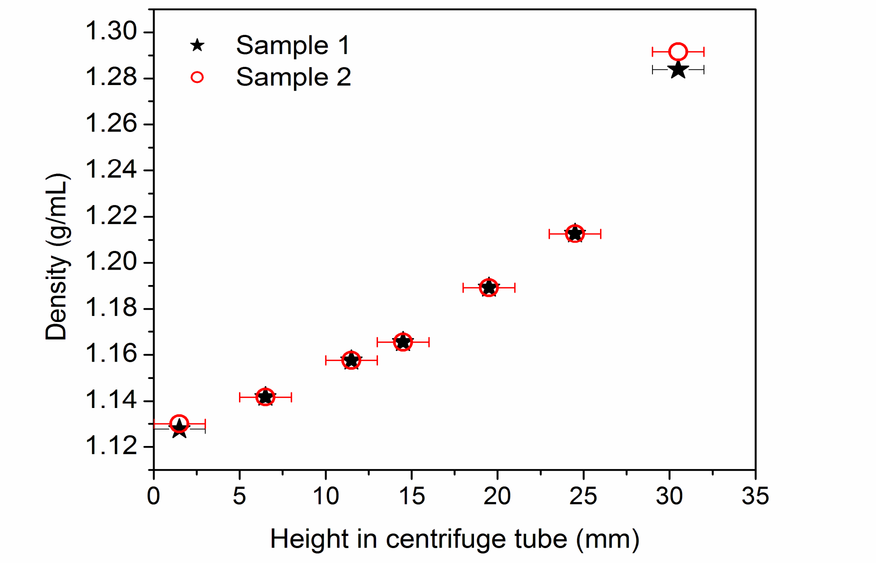

Figure S3: Densities of the different fractions (obtained from absorption) as a function of height in the centrifuge tube. A comparison is made between two different reference samples, presenting the reproducibility of the method.

3. Diffusion of the SWCNTs.

Time could be a very important factor for the *in situ* experiments. Immediately after the ultracentrifugation, diffusion of the SWCNTs is expected to destroy the separation. However, due to the large mass of SWCNTs their diffusion is very limited. To test this, we performed a RRS experiment (785nm) where we probe the position of empty and filled (9,7) tubes shortly after UCF (1 hour) and after leaving the sample diffuse for 24h. Slight diffusion can be observed as an increase of the Gaussian band width, but this is limited to only a 0.001g/mL shift in density after 24 hours. In addition, we observed a drift of all SWCNTs in the centrifuge tube, most probably due to creep of the plastic centrifuge tube after UCF (as it has expanded during UCF). However, the effect is extremely small (and constant for all SWCNTs), with only 0.004g/mL density shift after 24 hours.

Since experiments were performed in a time frame of maximum 6-10 hours after UCF, diffusion effects are thus minimal and within the experimentally determined error of 0.002g/mL. Diffusion of the gradient is much faster (smaller molecules) and therefore fractions for density calibration are collected immediately after each DGU run.

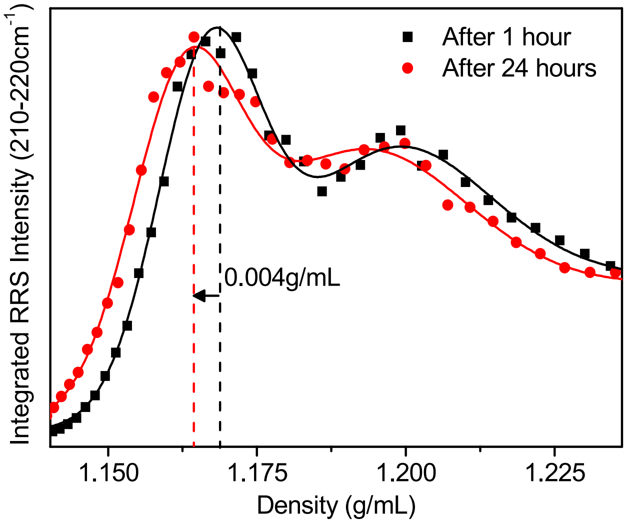

Figure S4: Integrated RRS intensity of a (9,7) SWCNT after separation (excitation wavelength = 785nm). The same spectrum (height) was acquired 1 hour and 25 hours after the ultracentrifugation. Diffusion of the SWCNTs leads to an increasing line width but is very slow: i.e. only a 0.001g/mL / 24 hours increase in Gaussian line width for the empty SWCNTs. We do observe a slight shift towards lower densities for all SWCNTs, which can be attributed to creep of the plastic centrifuge tube after ultracentrifugation, however this shift is very small, amounting to only 0.004g/mL after 24 hours.

4. *In situ* RRS experiments and fits at different excitation wavelengths

Unlike *in situ* PLE, i*n situ* RRS spectroscopy provides additional information on metallic SWCNTs, and those peculiar semiconducting SWCNTs that do not show fluorescence, *e.g.* the (5,3) chirality. Figures S4-S7 show a representative set of Raman data, measured at different excitation wavelengths (647.1nm, 785nm, 514.5nm and 725nm), in resonance with both metallic and semiconducting larger and smaller diameter SWCNTs.

The RRS data excited at 647.1nm are presented in two distinct regions, corresponding to larger diameter metallic SWCNTs (150-220cm^{-1}) and smaller diameter semiconducting SWCNTs (240-310cm^{-1}).

1D+1 RRS spectra were fitted using a combination of empty and filled peak positions for each chirality.

a) <u>647.1nm.</u>

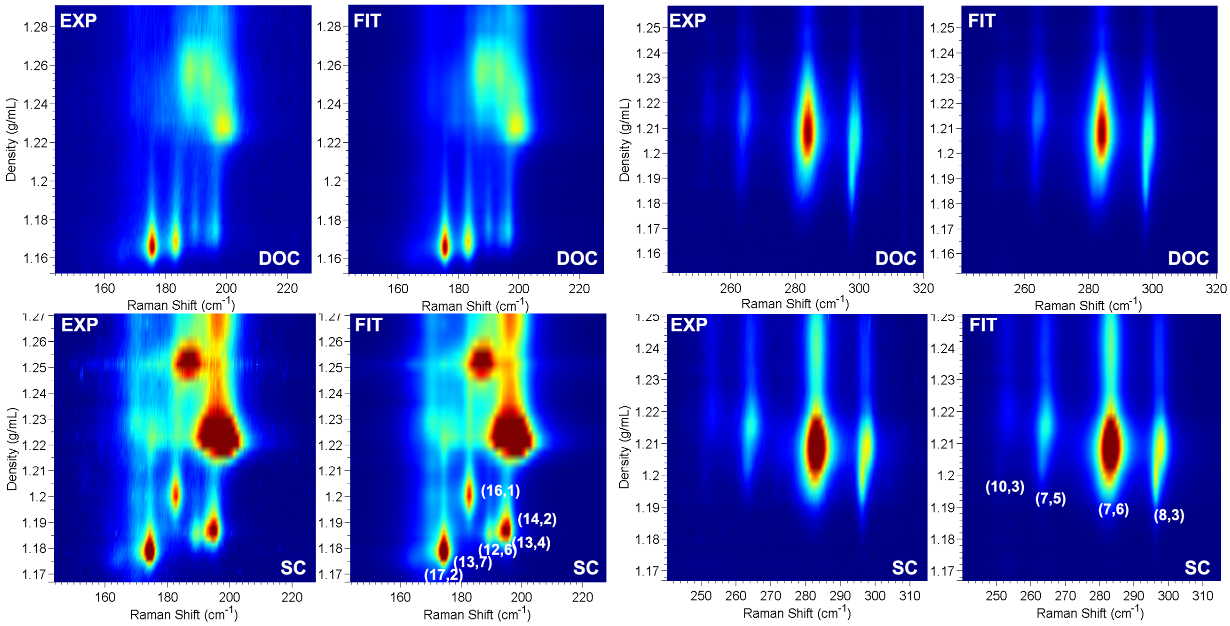

Figure S5: In situ RRS spectra and fits with excitation at 647.1nm, for 2% DOC (Top panels) and 2% SC (Bottom panels). Two distinct regions are fitted separately, corresponding to thicker and thinner diameter SWCNTs. From left to right the (17,2), (13,7), (16,1), (12,6), (13,4), (14,2), (10,3), (7,5), (7,6) and (8,3) tubes are fitted.

b) *785nm*

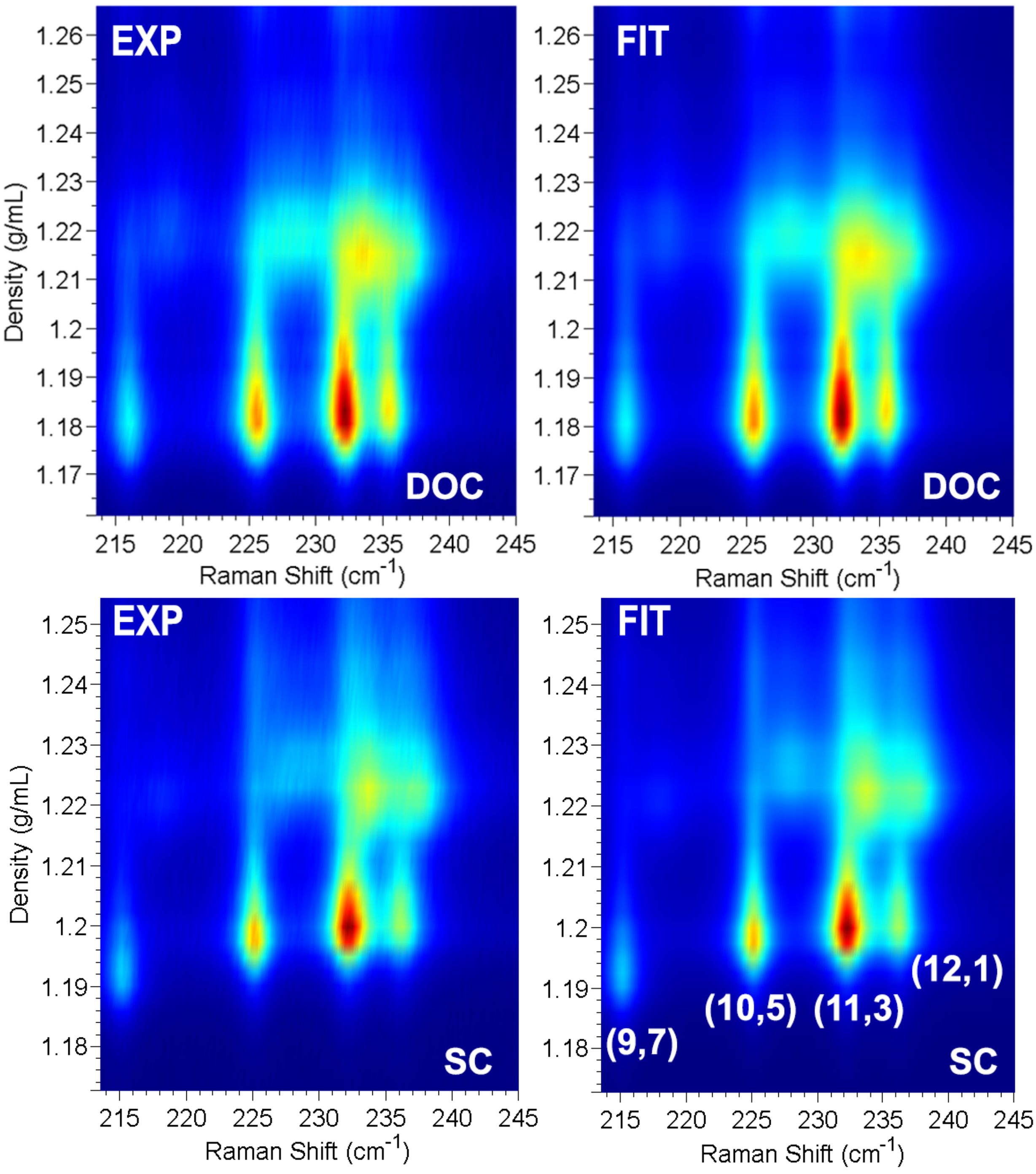

Figure S6: In situ RRS spectra and fits with excitation at 785nm, for 2% DOC (top panels) and 2% SC (bottom panels).. From left to right, the (9,7), (10,5), (11,3) and (12,1) tube are fitted

c) 514.5 nm

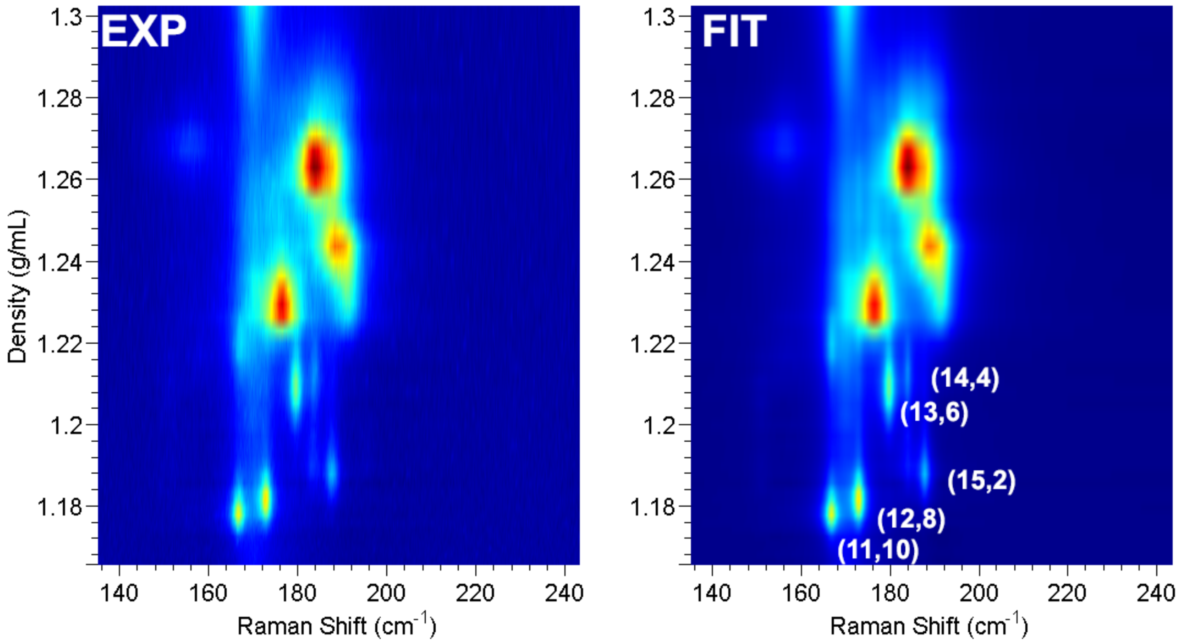

Figure S7: In situ RRS spectra (left) and fits (right) with excitation at 514.5 nm, for 2% SC. From left to right the (11,10), (12,8), (13,6), (14,4), (15,2) tubes.

d) 725 nm

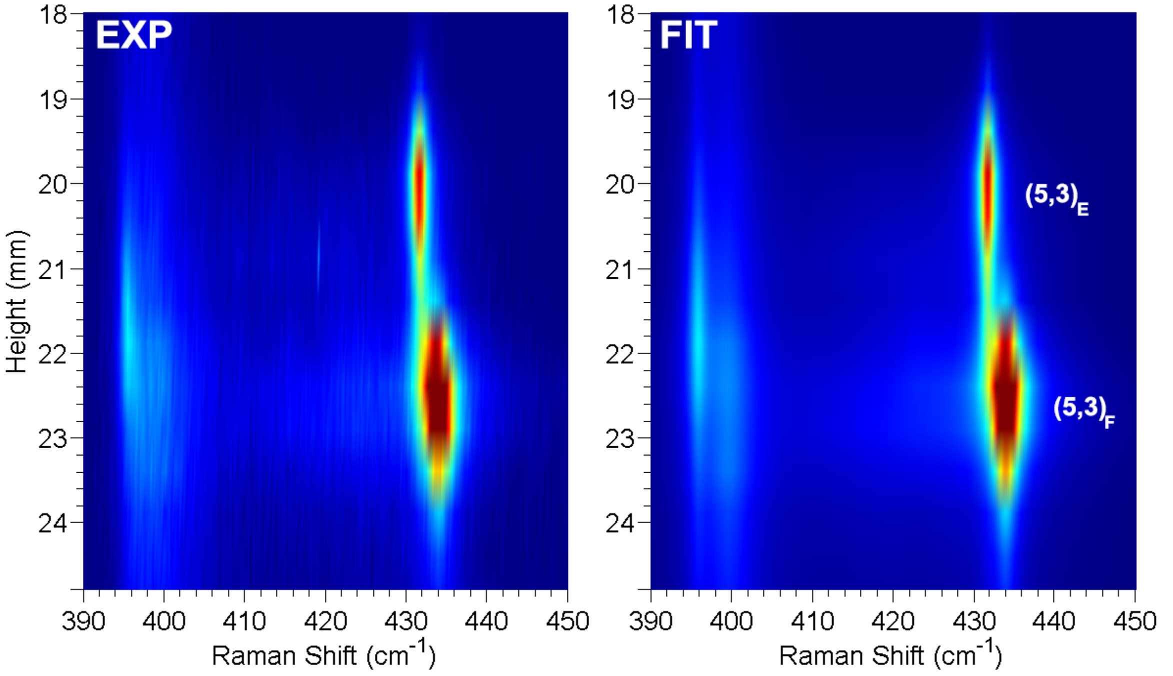

Figure S8: In situ RRS spectra (left) and fits (right) with excitation at 725nm, for 0.7% DOC, in resonance with the (5,3) tube. Also for this specific small diameter tube, empty (E) and filled (F) tubes can be clearly separated spectrally (as well as spatially) from each other.

5. Model fitting: Error analysis

The density and thickness of the surfactant layer that are determined by the model fit to the empty SWCNT densities (see Figure 7 and main text) are strongly correlated fit parameters, which needs to be taken into account to determine the error margins on these fit parameters, based on the full Jacobian of the χ^2. Therefore , we considered different approaches in deriving a properly defined χ^2: (1) One might simply weigh the experimental data points according to their respective experimental errors, yielding a χ^2-surface as presented by the blue contour plot in Figure S9. However, inspection of the fit (Figure 7) shows that the deviations due to chirality dependent variations of density (which are not included in the model) dominate over the actual experimental errors, so it is not appropriate to give undue additional weight to data points with smaller experimental errors. (2) The best estimate of density and thickness of the surfactant layer is thus rather obtained by giving the same weight to all data points. The green contours in Figure S9 show the resulting χ^2-surface when using a single, average experimental error. (3) To furthermore account for the systematic deviations due to the density variations for individual chiralities (not included in the concentric cylinder model, which only considers diameter), it is in this case more appropriate to normalize χ^2 based on these deviations rather than the *experimental* errors (red contours in Figure S9). The best fit values and correct (more conservative) error bars (1σ) which we have reported in the manuscript for density and thickness of the surfactant layer are thus determined by the last approach. Note however, that the alternative weighting schemes (albeit less appropriate) also yield fitted values within these conservative error bars.

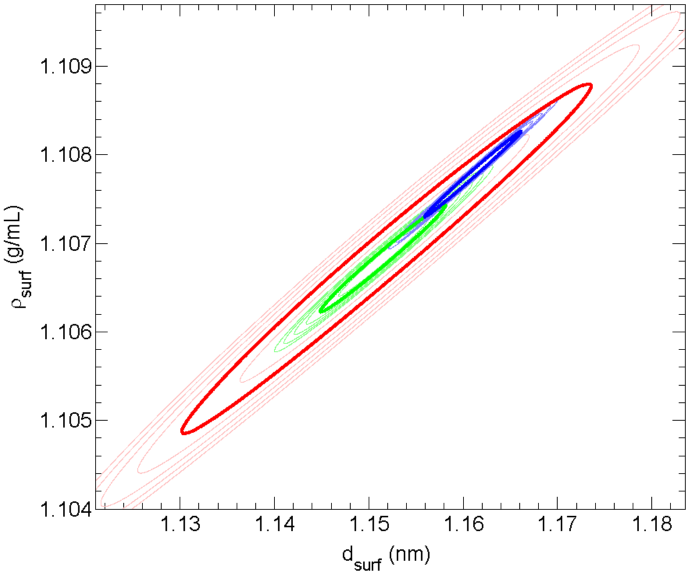

Figure S9. Contour plot of the χ^2 corresponding to the fit to the empty SWCNT data (orange curves in Figure 7). Contour lines are plotted at increments of 0.5 in χ^2, from the minimum χ^2 value (χ^2_{min}, i.e. best fit) up to χ^2_{min} +3, corresponding to 0.5σ through 3σ confidence levels on the fit parameters, with the 1σ contour represented by a bold curve. The colours represent the different weighting schemes considered (see text). The bold red curve corresponds to the 1σ error bars reported in the main text, and takes into account not only the experimental errors, but also the intrincic chirality dependent deviations from the simplified cylinder model (which is based on diameter only) which are larger.

6. Hard sphere model for the density of the encapsulated water

For the core density of the water-filled SWCNTs, we used the simple geometric model devised in reference 13, approximating the water molecules by hard spheres, closely packed in a hard cylinder, for which the analytical results by Pickett *et al.*[29] were used. For diameters larger than those for which analytical results have been obtained in reference [29], the volume fraction of the hard-sphere packing was extrapolated as $a+b/d$, such that at infinite diameter d, the volume fraction of a bulk close packing of spheres, $a=\pi/3\sqrt{2}$, is retrieved. Also as in reference [13], the density of the spheres was chosen such that this bulk close-packed arrangement corresponds to the density of bulk water, and the diameter of the cylinder was set to $d_{NT}-d_{wall}$, corresponding to the hollow core of the SWCNT. However, in reference [13], the diameter of the hard spheres was taken to be the distance between oxygen atoms in two water molecules connected by a hydrogen bond (d_{water}=0.29nm). That essentially described the longitudinal spacing of water molecules, but for describing the evolution of density with SWCNT diameter, it is rather the (lateral) size of the molecules (relative to the nanotube channel) which is more important. This size is smaller and known more precisely from the filling of small diameter tubes: water is experimentally known to enter thinner nanotubes down to the (5,3) SWCNT, with a diameter of 0.548nm and thus an inner core diameter of 0.208nm (and also theory predicts a critical diameter for filling close to this value).[26] We therefore now used this as a more accurate value for the effective sphere diameter (d_{water} =0.208nm). The resulting model density of the internal water as a function of SWCNT diameter (for both D_2O, as used here, and H_2O), is plotted in Figure S10.

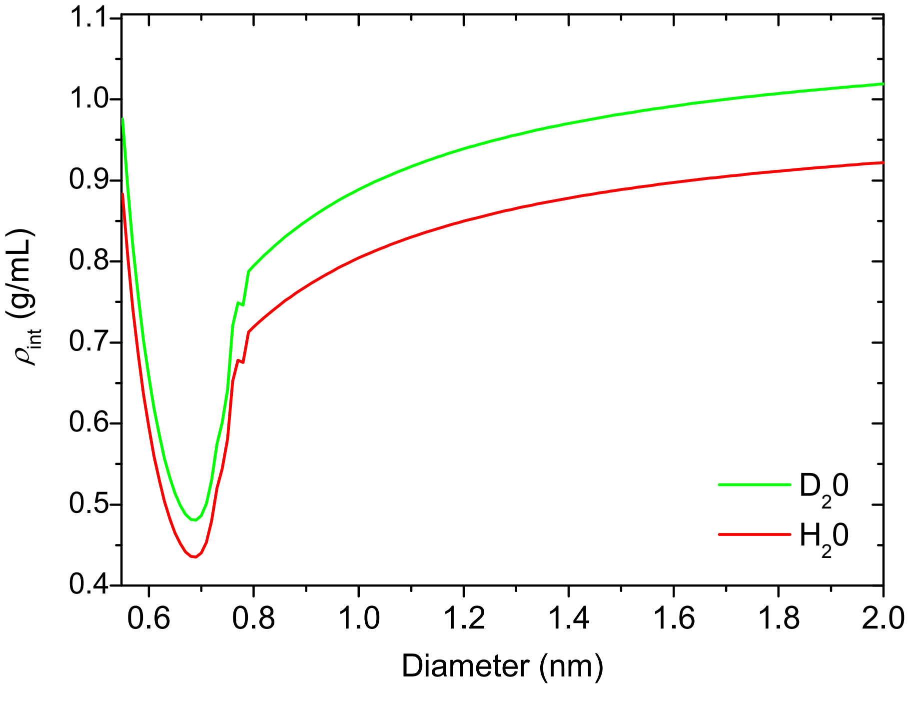

Figure S10. Density of the encapsulated water in water-filled SWCNTs as a function of SWCNT diameter, as calculated from the hard-spheres model using d_{water} =0.208nm (see text).